INTERNATIONAL JOURNAL FOR NUMERICAL METHODS IN ENGINEERING
Int. J. Numer. Meth. Engng 2003; **56**:935–960 (DOI: 10.1002/nme.592)

A reproducing kernel method with nodal interpolation property

Jiun-Shyan Chen[1,*,†], Weimin Han[2], Yang You[3] and Xueping Meng[2]

[1]*Department of Civil and Environmental Engineering, University of California, Los Angeles (UCLA), Los Angeles, CA 90095-1593, U.S.A.*
[2]*Department of Mathematics, The University of Iowa, Iowa City, IA 52242-1527, U.S.A.*
[3]*Department of Mechanical Engineering, The University of Iowa, Iowa City IA 52242-1527, U.S.A.*

SUMMARY

A general formulation for developing reproducing kernel (RK) interpolation is presented. This is based on the coupling of a primitive function and an enrichment function. The primitive function introduces discrete Kronecker delta properties, while the enrichment function constitutes reproducing conditions. A necessary condition for obtaining a RK interpolation function is an orthogonality condition between the vector of enrichment functions and the vector of shifted monomial functions at the discrete points. A normalized kernel function with relative small support is employed as the primitive function. This approach does not employ a finite element shape function and therefore the interpolation function can be arbitrarily smooth. To maintain the convergence properties of the original RK approximation, a mixed interpolation is introduced. A rigorous error analysis is provided for the proposed method. Optimal order error estimates are shown for the meshfree interpolation in any Sobolev norms. Optimal order convergence is maintained when the proposed method is employed to solve one-dimensional boundary value problems. Numerical experiments are done demonstrating the theoretical error estimates. The performance of the method is illustrated in several sample problems. Copyright © 2003 John Wiley & Sons, Ltd.

KEY WORDS: reproducing kernel approximation; reproducing kernel interpolation; meshfree method; essential boundary conditions; Kronecker delta properties

1. INTRODUCTION

Meshfree shape functions developed from moving least-squares (MLS) approximation [1–4], partition of unity [5–7], or reproducing kernel (RK) approximation [8–10] are in general not interpolation functions. Since the approximation spaces formed by these approximation functions are not kinematically admissible, a Lagrange multiplier method [2] or a penalty

*Correspondence to: Jiun-Shyan Chen, Department of Civil and Environmental Engineering, University of California, Los Angeles (UCLA), Los Angeles, CA 90095-1593, U.S.A.
†E-mail: jschen@seas.ucla.edu

Contract/grant sponsor: NSF/DARPA OPAAL; contract/grant number: DMS 98-74015
Contract/grant sponsor: Sandia National Laboratories; contract/grant number: 5015

Received 16 August 2001
Revised 1 February 2002
Accepted 11 April 2002

method [11] is required in the Galerkin framework to impose essential boundary conditions. Efforts have been devoted to construct kinematically admissible test and trial function spaces for Galerkin meshfree methods. A transformation method that transforms generalized co-ordinates to nodal co-ordinates for degrees of freedom associated with essential boundaries has been introduced [12], recovering nodal values by introducing singularity to the kernel functions has been discussed [13, 14], and employment of D'Alembert's principle in conjunction with co-ordinate transformation has also been proposed for essential boundary condition treatment [15].

Interpolation properties in finite elements can be recovered in meshfree approximation in numerous ways. Examples are coupling meshfree and finite element shape functions with a ramping in the transition zone [16], coupling and enrichment of finite element and meshfree shape functions via enforcement of reproducing conditions [17], and hierarchical enrichment of finite element solution using a meshfree approximation [18]. Rigorous convergence analysis and error estimation of this latter technique is given in Reference [19]. All these methods allow a direct imposition of essential boundary conditions, but require an underlined grid structure for construction of finite element shape functions. While attempts have been made to develop stabilized nodal integration methods [20–22] for integration of weak form, it is desirable to formulate a meshfree interpolation function that does not require an underlined grid.

In the method of enriching lower-order finite element solution by meshfree approximation [16], a set of finite element shape functions was first constructed in the designated sub-domains. Coupled MLS shape functions are then formed by imposing reproducing conditions. If finite element nodes are different from meshfree nodes, separate coefficients for finite element and meshfree shape functions are needed. In the case where the meshfree nodes coincide with the finite element nodes, the MLS approximation has to be at least one order higher than that of the intrinsic completeness of the FEM shape functions, and consequently, larger support sizes for MLS shape functions are necessary.

This work presents a general formulation for a meshfree approximation that recovers nodal values at designated points without the finite element enrichment. The proposed method follows the idea of coupling meshfree and finite element shape functions by Krongauz *et al*. [16] and Huerta *et al*. [17] but without using an underlying mesh. In the current approach the meshfree approximation constitutes a primitive function and an enrichment function. The requirement in the enrichment function for recovering interpolation properties in the reproducing kernel approximation is first identified. A simple normalized kernel function that does not cover any neighbour points is used as the primitive function. For the purpose of simplifying imposition of essential boundary conditions while maintaining the convergence properties of the regular RK approximation, a mixed interpolation is introduced. Primitive functions are only added to the essential boundary points so that the coefficients of meshfree approximation associated with the essential boundaries are nodal values.

In this paper, the RK approximation is reviewed in Section 2. The first part of Section 3 discusses the general requirements for obtaining interpolation properties in the enriched RK approximation, and the second part of this section presents specific forms of primitive function and enrichment functions. A mixed reproducing kernel interpolation (Mixed RKI) is also discussed in this section. Rigorous convergence analysis and error estimate of the proposed method are presented in Section 4, followed by numerical verifications in Section 5. Several example problems are given in Section 6 to evaluate the performance of the RK interpolation functions. Conclusions and remarks are given in Section 7.

2. REPRODUCING KERNEL APPROXIMATION

The approximation methods widely used in meshfree methods are the MLS approximation [1–4], partition of unity method (PUM) [5–7], and the RK approximation [8–10]. Since the reproducing conditions play an important role in the forthcoming discussion, the RK approximation is introduced in this section as the basis for developing meshfree interpolation functions.

To make the discussion general, we describe and analyse the method for an arbitrary d-dimensional problem, $d \geqslant 1$. For this purpose, we introduce some notations used in the rest of this paper. Let $\Omega \subset R^d$ be an nonempty, open bounded set with a Lipschitz continuous boundary. In the one-dimensional case, $d = 1$ and Ω is an open bounded interval. A generic point in R^d is denoted $\mathbf{x} = [x_1, \ldots, x_d]^{\mathrm{T}}$, or $\mathbf{y} = [y_1, \ldots, y_d]^{\mathrm{T}}$, or $\mathbf{z} = [z_1, \ldots, z_d]^{\mathrm{T}}$. We use the Euclidean norm to measure the vector length $\|\mathbf{x}\| = (\sum_{i=1}^{d} |x_i|^2)^{1/2}$. For $\mathbf{x}_0 \in R^d$ and $r > 0$, we denote $B_r(\mathbf{x}_0) = \{\mathbf{x} \in R^d \mid \|\mathbf{x} - \mathbf{x}_0\| \leqslant r\}$ for the closed ball with radius r centred at $\mathbf{x}_0$. In particular, when $\mathbf{x}_0 = \mathbf{0}$, we write B_r for $B_r(\mathbf{0})$. We use n for the highest degree of the polynomials that can be reproduced by the meshfree methods. Let $P_n = P_n(\Omega)$ be the space of the polynomials of degree $\leqslant n$ on Ω. The dimension of the space P_n is $N_n = (n + d)!/(n!d!)$.

It is convenient to use the multi-dimensional notation $\alpha = (\alpha_1, \ldots, \alpha_d)$ with $d \geqslant 0$ being integers. The quantity $|\alpha| = \sum_{i=1}^{d} \alpha_i$ is the length of α. This allows a simple notation for partial derivatives: $D^\alpha u(\mathbf{x}) = \partial^{|\alpha|} u(\mathbf{x}) / \partial x_1^{\alpha_1} \cdots \partial x_d^{\alpha_d}$. Denote $\alpha! = \alpha_1! \cdots \alpha_d!$ and $\mathbf{x}^\alpha = x_1^{\alpha_1} \cdots x_d^{\alpha_d}$.

Consider a problem domain $\bar{\Omega}$ discretized by a set of points $\{\mathbf{x}_I, \mathbf{x}_I \in \Omega\}_{I=1}^{NP}$. A function $u(\mathbf{x})$ defined in $\bar{\Omega}$ is approximated by

$$u^h(\mathbf{x}) = \sum_I \left[\sum_{|\alpha| \leqslant n} (\mathbf{x} - \mathbf{x}_I)^\alpha b_\alpha(\mathbf{x}) \right] \Phi_{a_I}(\mathbf{x} - \mathbf{x}_I) u_I \tag{1}$$

where $\{(\mathbf{x} - \mathbf{x}_I)^\alpha\}_{|\alpha| \leqslant n}$ is a set of monomial basis functions and $b_\alpha(\mathbf{x})$, $|\alpha| \leqslant n$, are the coefficients of the basis functions that vary with the location of approximation $\mathbf{x}$. The function $\Phi_{a_I}(\mathbf{x} - \mathbf{x}_I)$ is the kernel function centred at $\mathbf{x}_I$ that has a compact support $\omega_I = \mathrm{Supp}(\Phi_{a_I}(\mathbf{x} - \mathbf{x}_I)), \Phi_{a_I}(\mathbf{x} - \mathbf{x}_I) > 0$ for $\mathbf{x}$ in the interior of ω_I, and $\bigcup_I \omega_I \supset \Omega$. The support size a_I is a normalization parameter for distance measure so that $\Phi_{a_I}(\mathbf{x} - \mathbf{x}_I)$ vanishes when $\|\mathbf{x} - \mathbf{x}_I\|/a_I > 1$. For convenience, define the following notations:

$$\begin{aligned} \mathbf{H}^{\mathrm{T}}(\mathbf{x} - \mathbf{x}_I) &= \{(x - x_I)^\alpha\}_{|\alpha| \leqslant n} \\ &= \{1, x_1 - x_{1I}, \ldots, x_d - x_{dI}, (x_1 - x_{1I})^2, \ldots, (x_d - x_{dI})^n\} \end{aligned} \tag{2}$$

$$\begin{aligned} \mathbf{b}^{\mathrm{T}}(\mathbf{x}) &= \{b_\alpha(x)\}_{|\alpha| \leqslant n} \\ &= \{b_{0\cdots0}(\mathbf{x}), b_{10\cdots0}(\mathbf{x}), \ldots, b_{0\cdots01}(\mathbf{x}), b_{20\cdots0}(\mathbf{x}) \ldots, b_{00\cdots n}(\mathbf{x})\} \end{aligned} \tag{3}$$

and rewrite Equation (1) to

$$u^h(\mathbf{x}) = \sum_I \Psi_I(\mathbf{x}) u_I \tag{4}$$

$$\Psi_I(\mathbf{x}) = \mathbf{H}^{\mathrm{T}}(\mathbf{x} - \mathbf{x}_I) \mathbf{b}(\mathbf{x}) \Phi_{a_I}(\mathbf{x} - \mathbf{x}_I) \tag{5}$$

The coefficient vector $\mathbf{b}(\mathbf{x})$ is determined from the following reproducing conditions:

$$\sum_I \Psi_I(\mathbf{x})\mathbf{x}_I^\alpha = \mathbf{x}^\alpha, \quad |\alpha| \leqslant n \tag{6}$$

Equation (6) is equivalent to

$$\sum_I \Psi_I(\mathbf{x})(\mathbf{x} - \mathbf{x}_I)^\alpha = \delta_{|\alpha|,0}, \quad |\alpha| \leqslant n \tag{7}$$

or

$$\sum_I \Psi_I(\mathbf{x})\mathbf{H}(\mathbf{x} - \mathbf{x}_I) = \mathbf{H}(\mathbf{0}) \tag{8}$$

The $\mathbf{b}(\mathbf{x})$ vector is obtained by substituting Equation (5) into Equation (8) to yield

$$\mathbf{b}(\mathbf{x}) = \mathbf{M}^{-1}(\mathbf{x})\mathbf{H}(\mathbf{0}) \tag{9}$$

$$\mathbf{M}(\mathbf{x}) = \sum_I \mathbf{H}(\mathbf{x} - \mathbf{x}_I)\mathbf{H}^{\mathrm{T}}(\mathbf{x} - \mathbf{x}_I)\Phi_{a_I}(\mathbf{x} - \mathbf{x}_I) \tag{10}$$

Using Equations (5) and (9), function $\Psi_I(\mathbf{x})$ is obtained by

$$\Psi_I(\mathbf{x}) = \mathbf{H}^{\mathrm{T}}(\mathbf{0})\mathbf{M}^{-1}(\mathbf{x})\mathbf{H}(\mathbf{x} - \mathbf{x}_I)\Phi_{a_I}(\mathbf{x} - \mathbf{x}_I) \tag{11}$$

The function $\Psi_I(\mathbf{x})$ is called the RK approximation function or RK shape function. Note that for $\mathbf{M}(\mathbf{x})$ to be non-singular, the support of $\Phi_{a_I}(\mathbf{x} - \mathbf{x}_I)$ has to cover enough discrete points so that the reproducing conditions are satisfied at any location in the domain. This is referred to as the kernel stability and that is dependent on the order of reproducing conditions imposed. Conditions assuring the non-singularity of the matrix $\mathbf{M}(\mathbf{x})$ as well as good performance of the method are discussed in Reference [23], where rigorous convergence analysis and error estimates of the method are also provided.

3. REPRODUCING KERNEL INTERPOLATION

3.1. Modified reproducing kernel approximation

The RK shape functions discussed in Section 2 are in general not interpolation functions. This leads to complications in imposing essential boundary conditions and in applying nodal forces. It is therefore desirable to construct an interpolation function that preserves RK features. For this purpose, a modified RK approximation of $u(\mathbf{x})$ is considered as follows:

$$u^h(\mathbf{x}) = \sum_I \Psi_I(\mathbf{x})u_I \tag{12}$$

$$\Psi_I(\mathbf{x}) = \hat{\Psi}_I(\mathbf{x}) + \bar{\Psi}_I(\mathbf{x}) \tag{13}$$

In Equation (13), $\hat{\Psi}_I(\mathbf{x})$ is a primitive function used to introduce Kronecker delta properties in the approximation, and $\bar{\Psi}_I(\mathbf{x})$ is an enrichment function for imposing nth order reproducing conditions:

$$\sum_I [\hat{\Psi}_I(\mathbf{x}) + \bar{\Psi}_I(\mathbf{x})] x_I^\alpha = x^\alpha, \quad |\alpha| \leqslant n \tag{14}$$

In the following discussion, we will show that if $\hat{\Psi}_I(\mathbf{x}_J) = \delta_{IJ}$, and Equation (14) holds, then the vector of the enrichment functions, $\bar{\mathbf{\Psi}}(\mathbf{x}) = \{\bar{\Psi}_1(\mathbf{x}), \bar{\Psi}_2(\mathbf{x}), \ldots, \bar{\Psi}_{NP}(\mathbf{x})\}$, is orthogonal to the vector consisting of shifted monomial functions $\mathbf{h}_i(\mathbf{x}) = \{h_i(\mathbf{x}-\mathbf{x}_1), h_i(\mathbf{x}-\mathbf{x}_2), \ldots, h_i(\mathbf{x}-\mathbf{x}_{NP})\}$ where $h_i(\mathbf{x} - \mathbf{x}_I)$ is the ith component of $\mathbf{H}(\mathbf{x} - \mathbf{x}_I)$ in Equation (2), at all discrete points $\{\mathbf{x}_J\}_{J=1}^{NP}$, i.e.

$$\bar{\mathbf{\Psi}}(\mathbf{x}_J)^{\mathrm{T}} \mathbf{h}_i(\mathbf{x}_J) = 0 \quad \forall J \tag{15}$$

To show Equation (15), Equation (14) is first recast as

$$\sum_I [\hat{\Psi}_I(\mathbf{x}) + \bar{\Psi}_I(\mathbf{x})](\mathbf{x} - \mathbf{x}_I)^\alpha = \delta_{|\alpha|,0}, \quad |\alpha| \leqslant n \tag{16}$$

or

$$\sum_I [\hat{\Psi}_I(\mathbf{x}) + \bar{\Psi}_I(\mathbf{x})] \mathbf{H}(\mathbf{x} - \mathbf{x}_I) = \mathbf{H}(\mathbf{0}) \tag{17}$$

Evaluating Equation (17) at point $\mathbf{x}_J$ leads to

$$\sum_I [\bar{\Psi}_I(\mathbf{x}_J) + \hat{\Psi}_I(\mathbf{x}_J)] \mathbf{H}(\mathbf{x}_J - \mathbf{x}_I) = \mathbf{H}(\mathbf{0}) \tag{18}$$

If $\hat{\Psi}_I(\mathbf{x}_J) = \delta_{IJ}$, one has

$$\sum_I [\bar{\Psi}_I(\mathbf{x}_J) + \delta_{IJ}] \mathbf{H}(\mathbf{x}_J - \mathbf{x}_I) = \mathbf{H}(\mathbf{0}) \tag{19}$$

Since $\sum_I \delta_{IJ} \mathbf{H}(\mathbf{x}_I - \mathbf{x}_J) = \mathbf{H}(\mathbf{0})$ $\forall J$, Equation (19) reduces to

$$\sum_I \bar{\Psi}_I(\mathbf{x}_J) \mathbf{H}(\mathbf{x}_J - \mathbf{x}_I) = \mathbf{0} \tag{20}$$

or equivalently,

$$\sum_I \bar{\Psi}_I(\mathbf{x}_J) h_i(\mathbf{x}_J - \mathbf{x}_I) = 0 \tag{21}$$

This completes the proof of Equation (15). If indeed Equation (21) leads to a trivial solution $\bar{\Psi}_I(x_J) = 0$, then it follows that $\Psi_I(\mathbf{x})$ which satisfies reproducing condition in Equation (14) becomes an interpolation function. This can be achieved by considering the following formulation for $\bar{\Psi}_I(\mathbf{x})$:

$$\bar{\Psi}_I(\mathbf{x}) = \mathbf{G}^{\mathrm{T}}(\mathbf{x} - \mathbf{x}_I) \mathbf{a}(\mathbf{x}) \tag{22}$$

where $\mathbf{G}(\mathbf{x} - \mathbf{x}_I)$ is the vector of basis functions that has the same dimension as $\mathbf{H}(\mathbf{x} - \mathbf{x}_I)$, and $\mathbf{a}(\mathbf{x})$ is the corresponding coefficient vector. Substituting Equation (22) into Equation (20)

leads to

$$\mathbf{Q}(\mathbf{x}_J)\mathbf{a}(\mathbf{x}_J) = \mathbf{0} \tag{23}$$

where

$$\mathbf{Q}(\mathbf{x}) = \sum_I \mathbf{H}(\mathbf{x} - \mathbf{x}_I)\mathbf{G}^{\mathrm{T}}(\mathbf{x} - \mathbf{x}_I) \tag{24}$$

If $\mathbf{Q}(\mathbf{x}_J)$ is non-singular, Equation (24) yields a trivial solution $\mathbf{a}(\mathbf{x}_J) = \mathbf{0}$. It follows immediately $\bar{\Psi}_I(\mathbf{x}_J) = 0$ from Equation (22), and thus

$$\Psi_I(\mathbf{x}_J) = \bar{\Psi}_I(\mathbf{x}_J) + \hat{\Psi}_I(\mathbf{x}_J) = \delta_{IJ} \tag{25}$$

One obvious choice of $\mathbf{G}(\mathbf{x} - \mathbf{x}_I)$ for non-singular $\mathbf{Q}(\mathbf{x})$ is

$$\mathbf{G}(\mathbf{x} - \mathbf{x}_I) = \mathbf{H}(\mathbf{x} - \mathbf{x}_I)\bar{\Phi}_{\bar{a}_I}(\mathbf{x} - \mathbf{x}_I) \tag{26}$$

where $\bar{\Phi}_{\bar{a}_I}(\mathbf{x} - \mathbf{x}_I)$ is a positive function with compact support. Hence,

$$\bar{\Psi}_I(\mathbf{x}) = \mathbf{H}^{\mathrm{T}}(\mathbf{x} - \mathbf{x}_I)\mathbf{a}(\mathbf{x})\bar{\Phi}_{\bar{a}_I}(\mathbf{x} - \mathbf{x}_I) \tag{27}$$

Conclusion: If the enrichment function $\bar{\Psi}_I(\mathbf{x})$ takes the form of Equation (22), and the primitive function $\hat{\Psi}_I(\mathbf{x})$ has Kronecker delta properties, satisfaction of reproducing conditions in Equation (14) results in an interpolation function $\Psi_I(\mathbf{x})$.

The finite element shape functions is apparently a possible option for $\hat{\Psi}_I(\mathbf{x})$. This reduces to the approach of Huerta *et al.* [17]. In this paper, we consider the following simple construction of $\hat{\Psi}_I(\mathbf{x})$:

$$\hat{\Psi}_I(\mathbf{x}) = \frac{\hat{\Phi}_{\bar{a}_I}(\mathbf{x} - \mathbf{x}_I)}{\hat{\Phi}_{\hat{a}_I}(\mathbf{0})}, \quad \hat{a}_I < \min\{\|\mathbf{x}_I - \mathbf{x}_J\| \ \forall J \neq I\} \tag{28}$$

The support size $\hat{a}_I$ of $\hat{\Phi}_{\hat{a}_I}(\mathbf{x} - \mathbf{x}_I)$ is so chosen that it does not cover any neighbour points, and thus Kronecker delta conditions are satisfied in $\hat{\Psi}_I(\mathbf{x})$.

3.2. Reproducing conditions

Introducing Equations (27) and (28) into Equation (13), we obtain the coefficients $\mathbf{a}(\mathbf{x})$ in $\bar{\Psi}_I(\mathbf{x})$ by the reproducing condition:

$$\sum_I \left[\frac{\hat{\Phi}_{\hat{a}_I}(\mathbf{x} - \mathbf{x}_I)}{\hat{\Phi}_{\hat{a}_I}(\mathbf{0})} + \mathbf{H}^{\mathrm{T}}(\mathbf{x} - \mathbf{x}_I)\mathbf{a}(\mathbf{x})\bar{\Phi}_{\bar{a}_I}(\mathbf{x} - \mathbf{x}_I) \right] \mathbf{x}_I^{\alpha} = \mathbf{x}^{\alpha}, \quad |\alpha| \leqslant n \tag{29}$$

Equation (29) can be rewritten as

$$\sum_I \left[\frac{\hat{\Phi}_{\hat{a}_I}(\mathbf{x} - \mathbf{x}_I)}{\hat{\Phi}_{\hat{a}_I}(\mathbf{0})} + \mathbf{H}^{\mathrm{T}}(\mathbf{x} - \mathbf{x}_I)\mathbf{a}(\mathbf{x})\bar{\Phi}_{\bar{a}_I}(\mathbf{x} - \mathbf{x}_I) \right] (\mathbf{x} - \mathbf{x}_I)^{\alpha} = \delta_{|\alpha|,0}, \quad |\alpha| \leqslant n \tag{30}$$

or

$$\sum_I \mathbf{H}(\mathbf{x}-\mathbf{x}_I)\left[\frac{\hat{\Phi}_{\hat{a}_I}(\mathbf{x}-\mathbf{x}_I)}{\hat{\Phi}_{\hat{a}_I}(\mathbf{0})}+\mathbf{H}^{\mathrm{T}}(\mathbf{x}-\mathbf{x}_I)\mathbf{a}(\mathbf{x})\bar{\Phi}_{\bar{a}_I}(\mathbf{x}-\mathbf{x}_I)\right]=\mathbf{H}(\mathbf{0}) \tag{31}$$

The coefficient vector $\mathbf{a}(\mathbf{x})$ is obtained from Equation (31) by

$$\mathbf{a}(\mathbf{x})=\mathbf{Q}^{-1}(\mathbf{x})[\mathbf{H}(\mathbf{0})-\hat{\mathbf{F}}(\mathbf{x})] \tag{32}$$

$$\hat{\mathbf{F}}(\mathbf{x})=\sum_I \mathbf{H}(\mathbf{x}-\mathbf{x}_I)\frac{\hat{\Phi}_{\hat{a}_I}(\mathbf{x}-\mathbf{x}_I)}{\hat{\Phi}_{\hat{a}_I}(\mathbf{0})} \tag{33}$$

Finally, the RK interpolation function is obtained:

$$\Psi_I(\mathbf{x})=\frac{\hat{\Phi}_{\hat{a}_I}(\mathbf{x}-\mathbf{x}_I)}{\hat{\Phi}_{\hat{a}_I}(\mathbf{0})}+\mathbf{H}^{\mathrm{T}}(\mathbf{x}-\mathbf{x}_I)\mathbf{Q}^{-1}(\mathbf{x})[\mathbf{H}(\mathbf{0})-\hat{\mathbf{F}}(\mathbf{x})]\bar{\Phi}_{\bar{a}_I}(\mathbf{x}-\mathbf{x}_I) \tag{34}$$

It can be easily shown that

$$\begin{aligned}\Psi_I(\mathbf{x}_J)&=\frac{\hat{\Phi}_{\hat{a}_I}(\mathbf{x}_J-\mathbf{x}_I)}{\hat{\Phi}_{\hat{a}_I}(\mathbf{0})}+\mathbf{H}^{\mathrm{T}}(\mathbf{x}_J-\mathbf{x}_I)\mathbf{Q}^{-1}(\mathbf{x}_J)[\mathbf{H}(\mathbf{0})-\hat{\mathbf{F}}(\mathbf{x}_J)]\bar{\Phi}_{\bar{a}_I}(\mathbf{x}_J-\mathbf{x}_I)\\&=\delta_{IJ}+\mathbf{H}^{\mathrm{T}}(\mathbf{x}_J-\mathbf{x}_I)\mathbf{Q}^{-1}(\mathbf{x}_J)[\mathbf{H}(\mathbf{0})-\hat{\mathbf{F}}(\mathbf{x}_J)]\bar{\Phi}_{\bar{a}_I}(\mathbf{x}_J-\mathbf{x}_I)\end{aligned} \tag{35}$$

Since

$$\hat{\mathbf{F}}(\mathbf{x}_J)=\sum_I \mathbf{H}(\mathbf{x}_J-\mathbf{x}_I)\frac{\hat{\Phi}_{\hat{a}_I}(\mathbf{x}_J-\mathbf{x}_I)}{\hat{\Phi}_{\hat{a}_I}(0)}=\mathbf{H}(\mathbf{0}) \tag{36}$$

We have $\Psi_I(\mathbf{x}_J)=\delta_{IJ}$. Note that in Equations (35) and (36) the property $\hat{a}_I<\min\{\|\mathbf{x}_I-\mathbf{x}_J\|\ \forall J\neq I\}$ has been used.

For demonstration purposes, consider here the construction of a one-dimensional RK interpolation functions of a set of uniformly distributed discrete points with nodal distance $\Delta x = 0.1$. The two kernel functions are selected as $\bar{\Phi}_{\bar{a}_I}(x-x_I)=\phi((x-x_I)/\bar{a}_I)$ and $\hat{\Phi}_{\hat{a}_I}(x-x_I)=\phi((x-x_I)/\hat{a}_I)$, where ϕ is the cubic B-spline function, and $\bar{a}_I=2\Delta x$, and $\hat{a}_I=0.9\Delta x$. The two component functions $\bar{\Psi}_I(\mathbf{x})$ and $\hat{\Psi}_I(\mathbf{x})$, and combined RK interpolation function $\Psi_I(\mathbf{x})$ are shown in Figure 1. For irregular discretization, $\hat{a}_I$ should be carefully selected so that $\mathrm{Supp}(\hat{\Phi}_{\hat{a}_I})$ does not cover any neighbour points. A RK interpolation of one-dimensional irregular discretization is shown in Figure 2.

A representative discretization using RK interpolation functions is shown in Figure 3, where the supports with dash and solid lines refer to supports of $\hat{\Phi}_{\hat{a}_I}$ and $\bar{\Phi}_{a_I}$, respectively. Note that $\mathbf{x}_J\notin\mathrm{Supp}(\hat{\Phi}_{\hat{a}_I}(\mathbf{x}-\mathbf{x}_I))\ \forall J\neq I$.

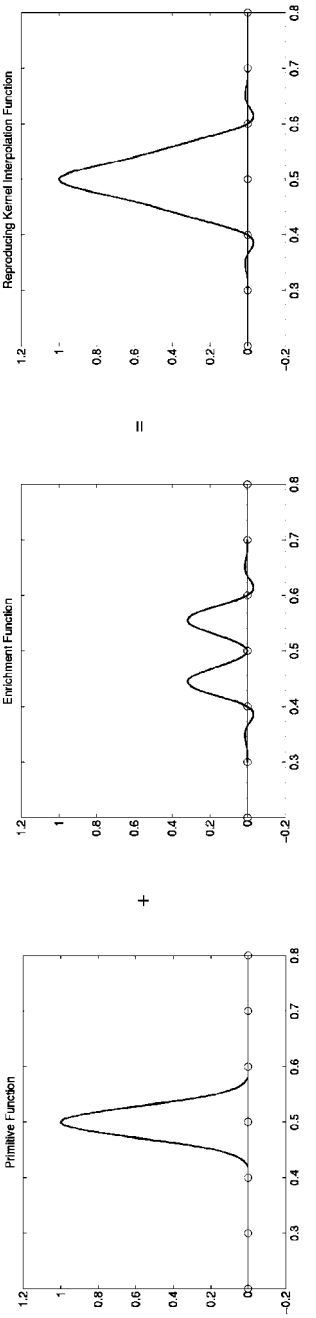

Figure 1. One-dimensional example of reproducing kernel interpolation function.

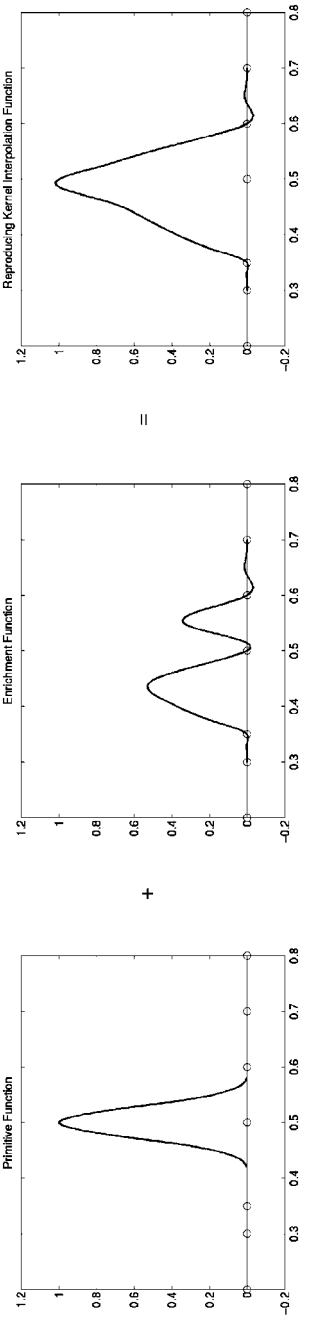

Figure 2. Reproducing kernel interpolation in one-dimensional irregular discretization.

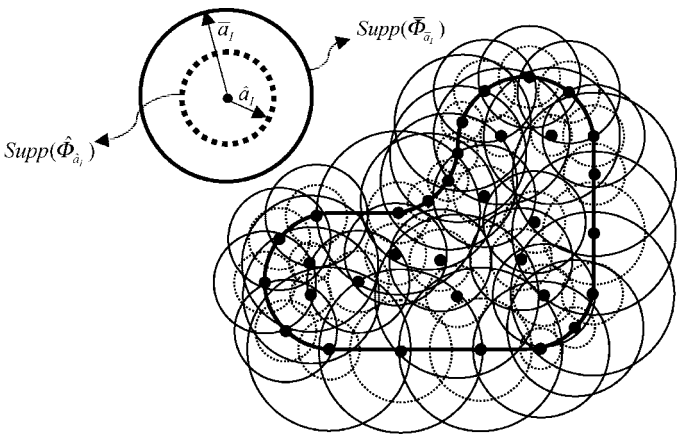

Figure 3. Domain discretization by reproducing kernel interpolation.

The RK interpolation function in Equation (34) bares the following properties:

1. The radius of $\mathrm{Supp}(\Psi_I(\mathbf{x}))$ is $\max(\bar{a}_I, \hat{a}_I)$.
2. If $\bar{\Phi}_{\hat{a}_I} \in C^{\bar{m}}$, $\hat{\Phi}_{\hat{a}_I} \in C^{\hat{m}}$, then $\Psi_I \in C^k$, $k = \min(\bar{m}, \hat{m})$.
3. The singularity of $\mathbf{Q}(\mathbf{x})$ is only dependent on $\bar{a}_I$ and the order of basis functions in $\mathbf{G}(\mathbf{x} - \mathbf{x}_I)$, and is independent to $\hat{a}_I$.
4. It is flexible to include primitive functions only for the designated points. For example, let the primitive function $\hat{\Psi}_K(\mathbf{x})$ be only included for point $\mathbf{x}_K$, i.e., $\Psi_I(\mathbf{x}) = \bar{\Psi}_I(\mathbf{x})$ for $I \neq K$, and $\Psi_K(\mathbf{x}) = \hat{\Psi}_K(\mathbf{x}) + \bar{\Psi}_K(\mathbf{x})$. Following Equations (34)–(36) it shows that $\Psi_K(\mathbf{x}_K) = 1$, and $\Psi_I(\mathbf{x}_K) = 0$ for all $I \neq K$. Note that $\Psi_K(\mathbf{x})$ does not vanish at other points, $\Psi_K(\mathbf{x}_I) \neq 0$. It is clear that in the approximation of $u(\mathbf{x})$ the nodal value of point $\mathbf{x}_K$ becomes the nodal value. For the purpose of a direct imposition of essential boundary conditions, the primitive functions can be added only to the essential boundary points. Figure 4 shows various conditions of including primitive functions in the construction of RK approximation: (a) no primitive function is included (traditional RK approximation), (b) primitive functions are added to all points, (c) primitive function is included only for a single point. We call case (c) of the RK approximation the mixed reproducing kernel interpolation, abbreviated as Mixed RKI in this paper.

As mentioned earlier, employment of finite element shape function for $\Psi_I(\mathbf{x})$ reduces RK interpolation to that of Huerta *et al.* [17]. However, this approach requires a finite element mesh for construction of finite element shape functions. It is also noted that since piecewise linear finite element shape functions possess linear completeness, at least second-order basis functions are needed in the construction of the enrichment function $\bar{\Psi}_I(\mathbf{x})$ in Reference [17]. Otherwise, $\bar{\Psi}_I(\mathbf{x}) \equiv 0$ and $\Psi_I(\mathbf{x}) \equiv N_I(\mathbf{x})$. This requires the increase of support size of $\bar{\Phi}_{\bar{a}_I}$ for non-singular $\mathbf{Q}(\mathbf{x})$, and that consumes higher computational effort in the construction of stiffness matrix and force vector. Further, $\Psi_I \in C^0$ in this case. The formulation proposed in this paper resolves this dilemma. Since the primitive function $\hat{\Psi}_I(\mathbf{x})$ does not possess the linear completeness, enrichment function $\bar{\Psi}_I(\mathbf{x})$ with the low order consistency will not vanish like that in FEM enrichment. Hence, smaller support size can be used for $\bar{\Phi}_{\bar{a}_I}(\mathbf{x} - \mathbf{x}_I)$ and arbitrary order of smoothness in Ψ_I can be obtained.

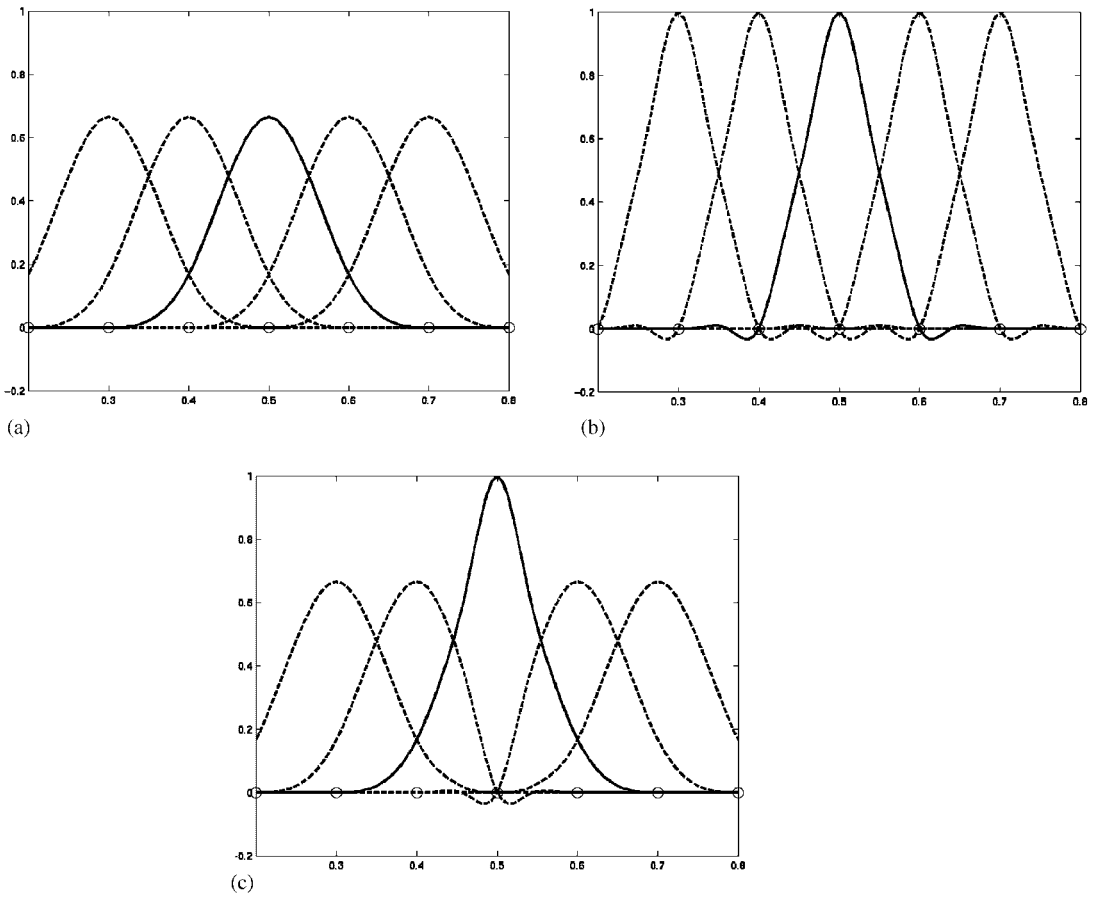

Figure 4. (a) Reproducing kernel approximation; (b) reproducing kernel interpolation; (c) mixed interpolation at single point.

4. ERROR ANALYSIS

For definiteness, we provide an error analysis of the proposed method when primitive functions are included only for the discrete points on the (relatively closed) part of the boundary $\Gamma_D \subset \partial\Omega$ where Dirichlet (essential) boundary conditions are specified. The case of including primitive functions for an arbitrarily chosen set of discrete points can be discussed with exactly the same technique. Let $\{\{\mathbf{x}_I\}_{I=1}^{NP}\} \subset \bar{\Omega}$ be a family of discrete point distributions. Thus, a continuous function $u \in C(\bar{\Omega})$ is approximated by

$$u(\mathbf{x}) \approx \sum_I \Psi_I(\mathbf{x}) u(\mathbf{x}_I) \tag{37}$$

The meshfree shape function is

$$\Psi_I(\mathbf{x}) = \begin{cases} \bar{\Psi}_I(\mathbf{x}) & \text{for } \mathbf{x}_I \notin \Gamma_D \\ \bar{\Psi}_I(\mathbf{x}) + \hat{\Psi}_I(\mathbf{x}) & \text{for } \mathbf{x}_I \in \Gamma_D \end{cases} \tag{38}$$

where $\hat{\Psi}_I(\mathbf{x})$ are the primitive functions and $\bar{\Psi}_I(\mathbf{x})$ are the enrichment functions

$$\bar{\Psi}_I(\mathbf{x}) = \mathbf{H}^{\mathrm{T}}(\mathbf{x} - \mathbf{x}_I)\mathbf{a}(\mathbf{x})\bar{\Phi}_{\bar{a}_I}(\mathbf{x} - \mathbf{x}_I) \tag{39}$$

with the coefficient function vector $\mathbf{a}(\mathbf{x}) \in R^{N_n}$ determined by reproducing conditions. For any $\mathbf{x}_I \in \Gamma_D$, the assumptions on $\hat{\Psi}_I$ are:

1. Supp($\hat{\Psi}_I$) does not contain $\mathbf{x}_J$ for $J \neq I$;
2. $\hat{\Psi}_I(\mathbf{x}_I) = 1$.

Then the Kronecker delta property holds for the particles on Γ_D:

$$\hat{\Psi}_I(\mathbf{x}_J) = \delta_{IJ}, \quad 1 \leqslant I \leqslant NP, \ \mathbf{x}_J \in \Gamma_D \tag{40}$$

We will derive error estimates for the case of quasiuniform support sizes, i.e.

$$c_1 \leqslant \frac{\bar{a}_I}{\bar{a}_J} \leqslant c_2 \quad \forall I, J \tag{41}$$

for two constants $0 < c_1 \leqslant c_2 < \infty$. Then there exists two constants $0 < \bar{c}_1 \leqslant \bar{c}_2 < \infty$ such that for any discrete point distribution $\{\mathbf{x}_I\}_{I=1}^{NP}$, we have a typical support size $\bar{a}$ and

$$\bar{c}_1 \leqslant \frac{\bar{a}_I}{\bar{a}} \leqslant \bar{c}_2 \quad \forall I \tag{42}$$

Now the polynomial reproducing condition

$$\sum_I \Psi_I(\mathbf{x})\mathbf{x}_I^{\alpha} = \mathbf{x}^{\alpha} \quad \forall \alpha: \ |\alpha| \leqslant n \tag{43}$$

is equivalent to

$$\sum_I \Psi_I(\mathbf{x})(\mathbf{x} - \mathbf{x}_I)^{\alpha} = \delta_{|\alpha|,0} \quad \forall \alpha: \ |\alpha| \leqslant n \tag{44}$$

This reproducing condition is rewritten as a linear system for the coefficient $a_\alpha(\mathbf{x})$:

$$\left[\sum_I \mathbf{H}(\mathbf{x} - \mathbf{x}_I)\mathbf{H}^{\mathrm{T}}(\mathbf{x} - \mathbf{x}_I)\bar{\Phi}_{\bar{a}_I}(\mathbf{x} - \mathbf{x}_I)\right]\mathbf{a}(\mathbf{x}) = \mathbf{H}(\mathbf{0}) - \sum_{\mathbf{x}_I \in \Gamma_D} \hat{\Psi}_I(\mathbf{x})\mathbf{H}(\mathbf{x} - \mathbf{x}_I) \tag{45}$$

Denote

$$\mathbf{M}_0(\mathbf{x}) = \sum_I \mathbf{H}\left(\frac{\mathbf{x} - \mathbf{x}_I}{\bar{a}}\right)\mathbf{H}^{\mathrm{T}}\left(\frac{\mathbf{x} - \mathbf{x}_I}{\bar{a}}\right)\bar{\Phi}_{\bar{a}_I}(\mathbf{x} - \mathbf{x}_I) \tag{46}$$

for the scaled moment matrix, and $\tilde{\mathbf{a}}(\mathbf{x}) = (\bar{a}^{|\alpha|}a_\alpha(\mathbf{x}))_{|\alpha| \leqslant n}$. Then the polynomial reproducing condition implies

$$\mathbf{M}_0(\mathbf{x})\tilde{\mathbf{a}}(\mathbf{x}) = \mathbf{H}(\mathbf{0}) - \sum_{\mathbf{x}_I \in \Gamma_D} \hat{\Psi}_I(\mathbf{x})\mathbf{H}\left(\frac{\mathbf{x} - \mathbf{x}_I}{\bar{a}}\right) \tag{47}$$

To describe conditions under which the method is defined and works well, we bring in some definitions. We say that a point $x \in \bar{\Omega}$ is covered by m shape functions if there are m indices $I_1, \ldots, I_m$ such that

$$\|\mathbf{x} - \mathbf{x}_{I_j}\| < \bar{a}_{I_j}, \quad j = 1, \ldots, m \tag{48}$$

We say a family of discrete point distributions $\{\{\mathbf{x}_I\}_{I=1}^{NP}\}$ is $(\bar{a}, n)$-regular if there is a constant L_0 such that

$$\max_{\mathbf{x} \in \bar{\Omega}} \|\mathbf{M}_0(\mathbf{x})^{-1}\|_2 \leqslant L_0 \tag{49}$$

for all the discrete point distributions in the family.

It can be shown that a family of one-dimensional discrete point distributions is $(\bar{a}, n)$-regular if any point is covered by at least $n+1$ shape functions and in any local region there are at least $n+1$ discrete points with relative distances bounded away from 0. For a general d-dimensional domain, a family of discrete point distributions is $(\bar{a}, 1)$-regular if any point is covered by $d+1$ shape functions and the d-simplex with the vertices of the corresponding discrete points has a volume larger than $\bar{c}_0 \bar{a}^d$. For details, see Reference [23].

In Equation (28), a concrete form for the primitive functions is suggested. For error analysis of the method, we make the following assumptions:

1. $\text{Supp}(\hat{\Psi}_I) = B(\mathbf{x}; \hat{a}_I)$ does not contain $\mathbf{x}_J$ for $J \neq I$.
2. There are constraints $0 < \hat{c}_1 \leqslant \hat{c}_2 < \infty$ such that $\hat{c}_1 \bar{a} \leqslant \hat{a}_I \leqslant \hat{c}_2 \bar{a}$ for any $x_I \in \Gamma_D$.
3. $\hat{\Psi}_I(\mathbf{x}_I) = 1$. (50)
4. $\hat{\Phi}_I \in C^k$.

By a standard scaling argument, we have the bounds

$$\max_{|\beta| = l} \|D^\beta \hat{\Psi}_I\|_{L^\infty(\Omega)} \leqslant c \bar{a}^{-l}, \quad l = 0, 1, \ldots, k \ \forall I \tag{51}$$

Notice that in the particular case of uniform discrete point distributions and uniform support sizes, we may simply take

$$\hat{\Psi}_I(\mathbf{x}) = \hat{\phi}\left(\frac{\mathbf{x} - \mathbf{x}_I}{\hat{a}}\right) \tag{52}$$

for some (fixed) function $\hat{\phi}$ with the properties:

1. $\text{Supp}(\hat{\phi}) = B(\mathbf{0}; c_0)$ is the ball centred at the origin with radius c_0 for any $c_0 \in (0, 1)$,
2. $\hat{\phi}(\mathbf{0}) = 1$, (53)
3. $\hat{\phi} \in C^k(\mathbf{B}(\mathbf{0}; c_0))$.

It is easy to see that the requirement Equation (50) on the functions $\hat{\Psi}_I$ are all satisfied with $\hat{c}_1 = \hat{c}_2 = 1$.

In the following, we always assume the regularity of the discrete point distributions. We also assume $\bar{\Phi} \in C^k$. From Equation (47) we immediately obtain

$$\max_{\alpha:|\alpha|\leqslant n} \bar{a}^{|\alpha|} \|a_\alpha\|_{L^\infty(\Omega)} \leqslant c \tag{54}$$

for some constant $c < \infty$.

Rewrite the enrichment functions (39) in the form

$$\bar{\Psi}_I(\mathbf{x}) = \mathbf{H}^{\mathrm{T}}\left(\frac{\mathbf{x}-\mathbf{x}_I}{\bar{a}}\right)\bar{\Phi}_{\bar{a}_I}(\mathbf{x}-\mathbf{x}_I)\bar{\mathbf{a}}^{|\alpha|}a_\alpha(\mathbf{x}) \tag{55}$$

Together with the bound Equation (51), we see that the meshfree shape functions are uniformly bounded:

$$\max_{1\leqslant I\leqslant NP} \|\Psi_I\|_{L^\infty(\Omega)} \leqslant c \tag{56}$$

We then bound the first derivatives of the shape functions. For any multi-index β with $|\beta| = 1$, we differentiate the system Equation (47) to obtain

$$\mathbf{M}_0(\mathbf{x})D^\beta\tilde{\mathbf{a}}(\mathbf{x}) = D^\beta\mathbf{M}_0(\mathbf{x})\tilde{\mathbf{a}}(\mathbf{x}) - \sum_{\mathbf{x}_I\in\Gamma_D}\left[D^\beta\hat{\Psi}_I(\mathbf{x})\mathbf{H}^{\mathrm{T}}\left(\frac{\mathbf{x}-\mathbf{x}_I}{\bar{a}}\right) + \hat{\Psi}_I(\mathbf{x})D^\beta\mathbf{H}^{\mathrm{T}}\left(\frac{\mathbf{x}-\mathbf{x}_I}{\bar{a}}\right)\right] \tag{57}$$

Using Equation (51), we know that the summation term on the right-hand side of Equation (57) is bounded by $c\bar{a}^{-1}$. Also, easily,

$$\max_{\beta:|\beta|=1}\max_{\mathbf{x}\in\bar{\Omega}} \|D^\beta\mathbf{M}_0(\mathbf{x})\|_2 \leqslant c\bar{a}^{-1} \tag{58}$$

Thus from Equation (57), we have

$$\max_{\beta:|\beta|=1}\max_{\alpha:|\alpha|\leqslant n} \bar{a}^{|\alpha|}\|D^\beta a_\alpha\|_{L^\infty(\Omega)} \leqslant c\bar{a}^{-1} \tag{59}$$

In general, an inductive argument shows that

$$\max_{\alpha:|\alpha|\leqslant n}\max_{\beta:|\beta|=l} \bar{a}^{|\alpha|}\|D^\beta a_\alpha\|_{L^\infty(\Omega)} \leqslant c\bar{a}^{-l}, \quad l = 0,1,\ldots,k \tag{60}$$

Then from Equation (55), we obtain the following result.

Theorem 4.1

Assume the discrete point distributions are $(\bar{a}, n)$-regular, $\bar{\Phi}$ is k-times continuously differentiable, and Equation (50) holds. Then

$$\max_I \max_{\beta:|\beta|=l} \|D^\beta\Psi_I\|_{L^\infty(\Omega)} \leqslant c\bar{a}^{-l}, \quad 0\leqslant l\leqslant k \tag{61}$$

Now we are ready to derive error estimates for the meshfree interpolants. For this purpose, we first introduce some definitions. Let $B \subset R^d$ be a ball. Then a domain Ω_1 is said to be star-shaped with respect to B if for any $\mathbf{x} \in \Omega_1$, the closed convex hull of $\{\mathbf{x}\} \cup B$ is a subset of Ω_1.

The chunkiness parameter of Ω_1 is defined to be $\Omega_1/\rho_{\max}$, where

$$\rho_{\max} = \sup\{\rho\colon\ \Omega_1 \text{ is star-shaped with respect to a ball of radius } \rho\} \tag{62}$$

Let $u \in W^{m+1,q}(\Omega)$, $m \geqslant 0$, $q \in [1,\infty]$. We assume $(m+1)q > d$ if $q > 1$, or $m+1 \geqslant d$ if $q = 1$. Then by the Sobolev embedding theorem, $u \in C(\bar{\Omega})$, and it is meaningful to use pointwise values of $u(\mathbf{x})$. The meshfree interpolant of $u(\mathbf{x})$ is

$$u^I(\mathbf{x}) = \sum_I u(\mathbf{x}_I)\Psi_I(\mathbf{x}), \quad \mathbf{x} \in \bar{\Omega} \tag{63}$$

Notice that this function interpolates u at the discrete points on the essential boundary: $u^I(\mathbf{x}_I) = u(\mathbf{x}_I)$ for $\mathbf{x}_I \in \Gamma_D$. Denote $n_1 = \min\{m+1, n+1\}$.

We will assume the following hypothesis is satisfied.

Hypothesis (H)
There is a constant integer N_0 such that for any $\mathbf{x} \in \bar{\Omega}$, there are at most N_0 of $\mathbf{x}_I$ satisfying the relation $\|\mathbf{x} - \mathbf{x}_I\| < \bar{a}_I$, i.e., each point in $\bar{\Omega}$ is covered by at most N_0 shape functions.

Hypothesis (H) is quite natural since otherwise as the number of shape functions covering a local area increases, the shape functions tend to be more and more linearly dependent in the local area.

To simplify the notation, we write $B_I \equiv B_{\bar{a}_I}(\mathbf{x}_I)$, $1 \leqslant I \leqslant NP$. We first bound the error $u - u^I$ in Sobolev norms over $B_J \cap \bar{\Omega}$ for $J = 1, \ldots, NP$. Define

$$\Omega_J = \left\{\mathbf{x}\colon\ \|\mathbf{x} - \mathbf{x}_J\| < \bar{a}_J + \max_{1 \leqslant I \leqslant NP} \bar{a}_I\right\} \tag{64}$$

and let

$$S_J = \{I\colon\ \operatorname{dist}(\mathbf{x}_I, B_J) < \bar{a}_I\} \tag{65}$$

It follows from hypothesis (H) that card (S_J), $1 \leqslant I \leqslant NP$, are uniformly bounded. If $\bar{\Omega}_J \subset \bar{\Omega}$, then $\bar{\Omega}_J \cap \bar{\Omega} = \bar{\Omega}_J$ is star-shaped with respect to $\tilde{B}_J \equiv B_J$, and the chunkiness parameter of $\bar{\Omega}_J \cap \bar{\Omega}$ is uniformly bounded. Now suppose $\bar{\Omega}_J \not\subset \bar{\Omega}$. Then since $\partial\Omega$ is Lipschitz continuous, if $\bar{a}$ is sufficiently small, we can choose a ball $\tilde{B}_J$ of radius $\bar{a}_J/2$ with $\mathbf{x}_J$ on its boundary such that $\bar{\Omega}_J \cap \bar{\Omega}$ is star-shaped with respect to $\tilde{B}_J$. Again we see that the chunkiness parameter of $\bar{\Omega}_J \cap \bar{\Omega}$ is uniformly bounded.

Let $P_J^{n_1} u$ be the Taylor polynomial of degree $n_1 - 1$ of u averaged over $\tilde{B}_J$ [24, Section 4.1], and denote

$$R_J^{n_1} u(\mathbf{x}) = u(\mathbf{x}) - P_J^{n_1} u(\mathbf{x}) \tag{66}$$

for the remainders. Then since the chunkiness parameters of $\bar{\Omega}_J \cap \bar{\Omega}$ are uniformly bounded when $\bar{a}$ is sufficiently small, from the results of [24, Section 4.3], we have the estimates:

$$\|R_J^{n_1} u\|_{W^{l,q}(\Omega_J \cap \Omega)} \leqslant c\bar{a}^{n_1 - l} |u|_{W^{n_1,q}(\Omega_J \cap \Omega)}, \quad l = 0, \ldots, n_1 \tag{67}$$

$$\|R_J^{n_1} u\|_{L^\infty(\Omega_J \cap \Omega)} \leqslant c\bar{a}^{n_1 - d/q} |u|_{W^{n_1,q}(\Omega_J \cap \Omega)} \tag{68}$$

where the constant c depends only on n_1, d and q, and is independent of J.

For $x \in B_J \cap \bar{\Omega}$, we have

$$u(\mathbf{x}) - u^I(\mathbf{x}) = P_J^{n_1} u(\mathbf{x}) - \sum_I P_J^{n_1} u(\mathbf{x}_I)\Psi_I(\mathbf{x}) + R_J^{n_1} u(\mathbf{x}) - \sum_{I \in S_J} R_J^{n_1} u(\mathbf{x}_I)\Psi_I(\mathbf{x}) \tag{69}$$

By the polynomial reproducing property,

$$\sum_I P_J^{n_1} u(\mathbf{x}_I)\Psi_I(\mathbf{x}) = P_J^{n_1} u(\mathbf{x}) \tag{70}$$

Thus we have the error representation formula

$$u(\mathbf{x}) - u^I(\mathbf{x}) = R_J^{n_1} u(\mathbf{x}) - \sum_{I \in S_J} R_J^{n_1} u(\mathbf{x}_I)\Psi_I(\mathbf{x}) \tag{71}$$

Note that $\mathbf{x}_I \in \bar{\Omega}_J \cap \bar{\Omega}$ for $I \in S_J$. So

$$\|u - u^I\|_{W^{l,q}(B_J \cap \Omega)} \leqslant \|R_J^{n_1} u\|_{W^{l,q}(B_J \cap \Omega)} + \|R_J^{n_1} u\|_{L^\infty(\Omega_J \cap \Omega)} \sum_{I \in S_J} \|\Psi_I\|_{W^{l,q}(B_J \cap \Omega)} \tag{72}$$

Since $\mathrm{card}(S_J)$ is uniformly bounded, applying estimates (67), (68) and Theorem 4.1, we have

$$\|u - u^I\|_{W^{l,q}(B_J \cap \Omega)} \leqslant c\bar{a}^{n_1 - l}|u|_{W^{n_1,q}(\Omega_J \cap \Omega)}, \quad 0 \leqslant l \leqslant \min\{n_1, k\}, \ 1 \leqslant J \leqslant NP \tag{73}$$

Therefore, recalling again hypothesis (H),

$$\|u - u^I\|_{W^{l,q}(\Omega)} \leqslant c\bar{a}^{n_1 - l}|u|_{W^{n_1,q}(\Omega)}, \ 0 \leqslant l \leqslant \min\{n_1, k\} \tag{74}$$

To conclude, we have derived the following optimal order meshfree interpolation error estimates.

Theorem 4.2
Assume the conditions stated in Theorem 4.1. Also assume hypothesis (H). Let $m \geqslant 0$, $q \in [1, \infty]$ with $(m+1)q > d$ if $q > 1$, or $m + 1 \geqslant d$ if $q = 1$. Then for any $u \in W^{m+1,q}(\Omega)$, we have the optimal order interpolation error estimates

$$\|u - u^I\|_{W^{l,q}(\Omega)} \leqslant c\bar{a}^{\min\{m+1, n+1\} - l}|u|_{W^{\min\{m+1, n+1\},q}(\Omega)} \quad \forall l \leqslant \min\{m+1, n+1, k\} \tag{75}$$

Notice that when u is sufficiently smooth, $m \geqslant n$, the error estimate Equation (75) reduces to

$$\|u - u^I\|_{W^{l,q}(\Omega)} \leqslant c\bar{a}^{n+1-l}|u|_{W^{n+1,q}(\Omega)} \quad \forall l \leqslant \min\{n+1, k\} \tag{76}$$

If we further assume $\bar{\Phi}$ and $\hat{\Psi}_I$ are sufficiently smooth so that $k \geqslant n+1$, then

$$\|u - u^I\|_{W^{l,q}(\Omega)} \leqslant c\bar{a}^{n+1-l}|u|_{W^{n+1,q}(\Omega)}, \quad l = 0, 1, \ldots, n+1 \tag{77}$$

For meshfree solutions u^R of one-dimensional elliptic boundary value problems, it then follows that the optimal order error estimates hold:

$$\|u - u^R\|_{H^1(\Omega)} \leqslant c\bar{a}^n |u|_{H^{n+1}(\Omega)} \tag{78}$$

5. CONVERGENCE STUDY

In this section, we present some results on numerical experiments of the meshfree methods to demonstrate the theoretical error estimates derived in the previous section. Numerical examples showing the performance of the proposed method will be given in the next section.

For all the following numerical experiments, we use uniform discrete point distributions and uniform support sizes. Then the support size $\bar{a}$ is proportional to the nodal distance h. From the results of the previous section, we have the following error estimates for the meshfree interpolant u^I:

$$\|u - u^I\|_{H^1(\Omega)} \leqslant ch^n |u|_{H^{n+1}(\Omega)} \tag{79}$$

$$\|u - u^I\|_{L^2(\Omega)} \leqslant ch^{n+1} |u|_{H^{n+1}(\Omega)} \tag{80}$$

as long as the function u belongs to the space $H^{n+1}(\Omega)$. For a one-dimensional linear elliptic boundary value problem, we also have the optimal order meshfree error estimate of meshfree solution u^R:

$$\|u - u^R\|_{H^1(\Omega)} \leqslant ch^n |u|_{H^{n+1}(\Omega)} \tag{81}$$

By the well-known Nitsche's technique, we also have the optimal order meshfree error estimate in L^2 norm:

$$\|u - u^R\|_{L^2(\Omega)} \leqslant ch^{n+1} |u|_{H^{n+1}(\Omega)} \tag{82}$$

Two examples are analysed to verify the order of convergence. The first example is a one-dimensional boundary value problem:

$$\begin{aligned} u_{,xx} &= e^x, \quad x \in (0,1) \\ u(0) &= 1, \quad u(1) = e \end{aligned} \tag{83}$$

The exact solution is $u(x) = e^x$. Uniform particle distributions and uniform support sizes are used for meshfree computation. Denote h the distance between two neighbouring particles and n the polynomial degree. The support size of the enrichment functions is chosen as $\bar{a}/h = 2.1 + n$, and that of the primitive functions $\hat{a}/h = 0.5$. Figure 5 shows errors of RK interpolations and Figure 6 the errors of meshfree solutions in L^2 related norms. Essential boundary conditions are imposed using the Kronecker delta property of RK interpolation on the essential boundaries. We observe the optimal-order convergence for both the meshfree interpolants and the meshfree solutions. By comparison of numerical solution using $\hat{a}/h = 0.1, 0.5, 0.9$, the results show that the support size of primitive function $\hat{a}$ has very minimum influence on the solution accuracy and the order of convergence.

For the two-dimensional boundary value problem, we solve the following Poisson equation:

$$\begin{aligned} \nabla^2 u(x,y) &= (x^2 + y^2) e^{xy} \quad (x,y) \in (0,1) \times (0,1) \\ u(0,y) &= 1, \quad u(1,y) = e^y, \quad 0 \leqslant y \leqslant 1 \\ u(x,0) &= 1, \quad u(x,1) = e^x, \quad 0 \leqslant x \leqslant 1 \end{aligned} \tag{84}$$

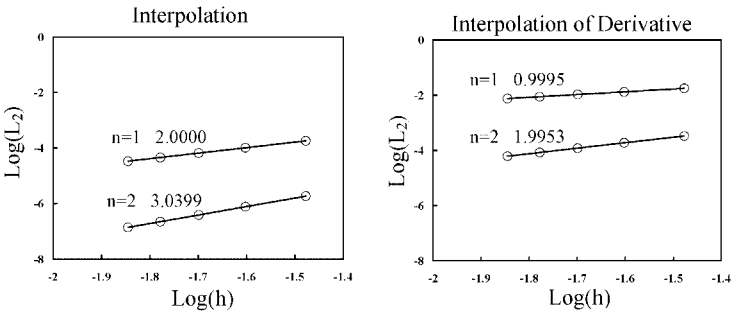

Figure 5. Error norms of one-dimensional reproducing kernel interpolation.

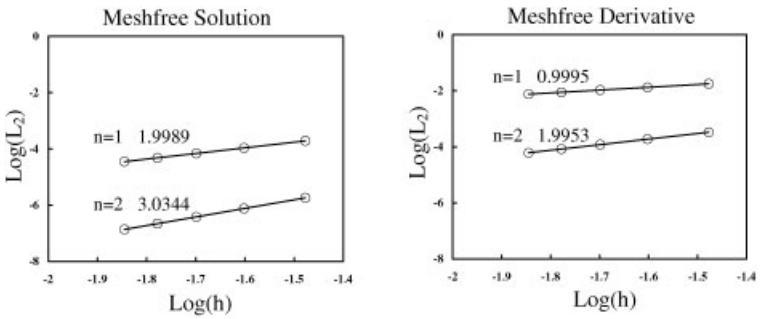

Figure 6. Error norms of one-dimensional meshfree solution.

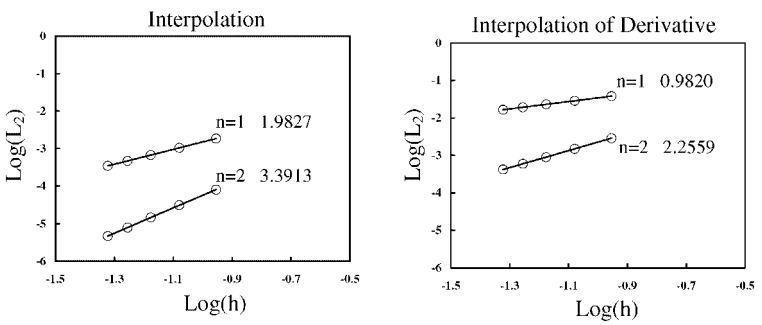

Figure 7. Error norms of two-dimensional reproducing kernel interpolation.

The exact solution is $u(x, y) = e^{xy}$. Uniform particle distributions and uniform support sizes are used for meshfree computation. Denote h the distance in the x or y direction between two neighbouring particles and n the monomial degree. The support size of the enrichment functions is chosen as $\bar{a}/h = 2.1 + n$, and that of the primitive functions $\hat{a}/h = 0.5$. Numerical results shown in Figure 7 indicate that we have optimal order convergence for the RK interpolation. Meshfree solution using first-order monomials shown in Figure 8 also achieves

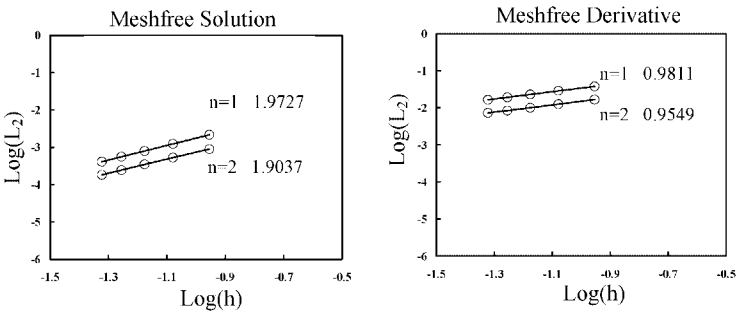

Figure 8. Error norms of two-dimensional meshfree solution.

optimum order of convergence. For higher monomial degrees, although the convergence order in the energy norm is still one, the corresponding meshfree solutions are more accurate than that with linear basis functions. This is due to the fact that the essential boundary conditions are imposed only at discrete points. Similar phenomenon was observed in the meshfree solution using standard RK approximation.

6. NUMERICAL EXAMPLES

In the following examples, unless otherwise specified, mixed reproducing kernel interpolation (Mixed RKI) functions using cubic B-spline kernel with linear basis are employed. Normalized support sizes for $\bar{\Phi}_{\bar{a}_I}$ and $\hat{\Phi}_{\hat{a}_I}$ are defined as $\bar{R}_I = \bar{a}_I/h$ and $\hat{R}_I = \hat{a}_I/h$, where h is the nodal distance.

6.1. One-dimensional equation

In this example, the following model problem is considered:

$$\begin{aligned} -u_{,xx} + 20u(x) &= 0 \quad \text{in } (0,1) \\ u(0) &= c_1, u(1) = c_1 \exp(\sqrt{20}) + c_2 \exp(-\sqrt{20}) \end{aligned} \tag{85}$$

where $c_1 = 1/(\exp(\sqrt{20}) - \exp(-\sqrt{20}))$, $c_2 = c_1 - 1/\sqrt{20}$, RK interpolation functions are constructed using linear basis functions with normalized support size $\hat{R}_I = 0.9$ for $\hat{\Phi}_{\hat{a}_I}$ and $\bar{R}_I = 2.0$ for $\bar{\Phi}_{\bar{a}_I}$. The solution is also compared with the regular RK approximation with boundary conditions imposed by Lagrange multiplier method. The comparison of u and $\mathrm{d}u/\mathrm{d}x$ with an equally spaced 11-node model is shown in Figure 9.

The convergence of the proposed formulation with respect to the support size of the interpolation function is also studied. For this purpose $\bar{R}_I = 1.2, 2.0, 3.0$ for $\bar{\Phi}_{\bar{a}_I}$ are considered in the analysis. Consecutively refined regular models with 11, 21, 41, and 81 points are used in the convergence study. The error norms in u and $\mathrm{d}u/\mathrm{d}x$ are plotted in Figure 10. The results show a characteristic similar to that of the conventional RK approximation.

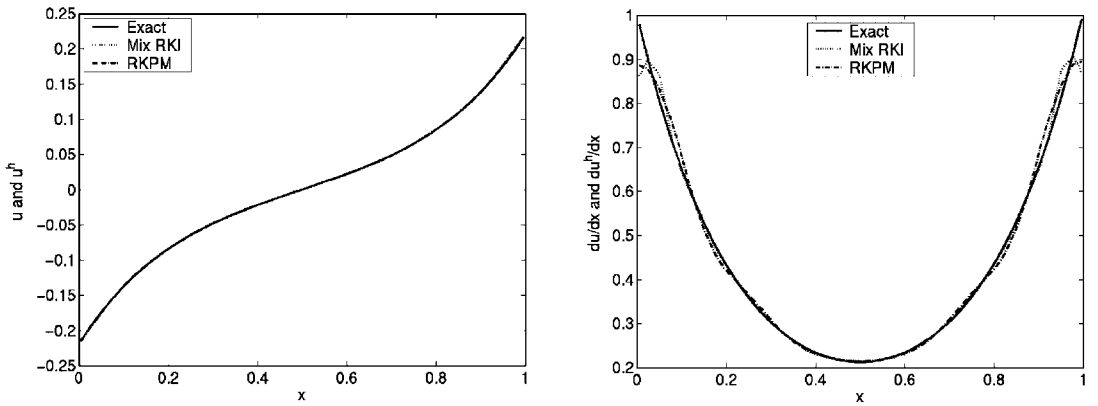

Figure 9. Solution comparison using 11 nodes regular model.

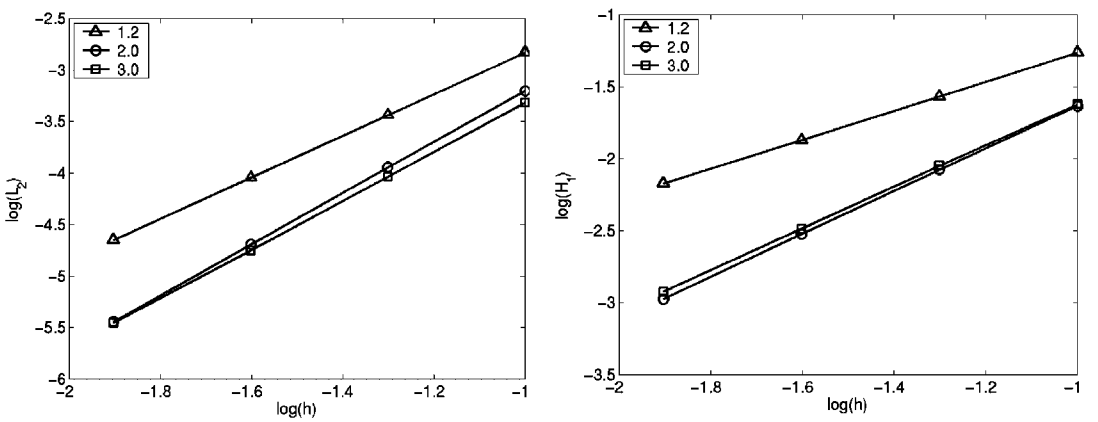

Figure 10. Error norms in u and $\mathrm{d}u/\mathrm{d}x$ for $\bar{R}_I = 1.2, 2.0, 3.0$.

6.2. *Beam bending*

A cantilever beam subjected to a shear load as shown in Figure 11 is studied. Owing to the symmetry in the geometry, only half of the model 1s modelled. Three regular models with 11×3, 21×5, and 41×9 points, as shown in Figure 12, are tested. Linear basis functions with normalized support sizes $\hat{R}_I = 0.9$ for $\hat{\Phi}_{\hat{a}_I}$ and $\bar{R}_I = 2.0$ for $\bar{\Phi}_{\bar{a}_I}$ are employed. The comparison of Mixed RKI, the regular RK approximation, and the finite element solution are shown in Table I. It is noted that with the Mixed RKI, the imposition of essential boundary conditions is much less costly than that of the regular RK approximation with Lagrange multiplier method.

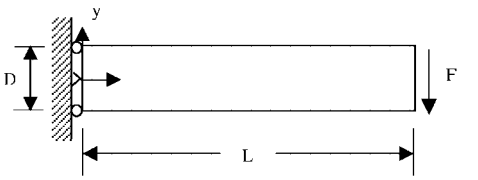

Figure 11. Beam bending problem configuration.

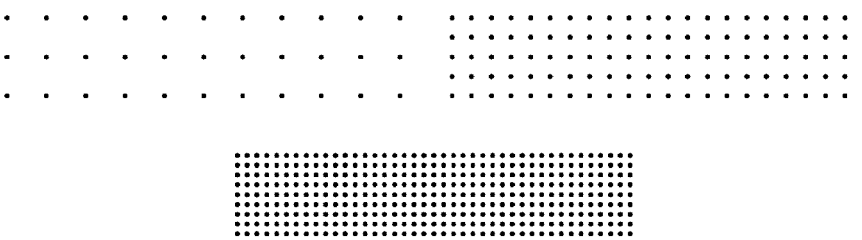

Figure 12. Regular models with 11×3, 21×5, and 41×9 nodes.

Table I. Tip displacement comparison in beam problem.

Model	33	105	369
FEM	71.1956%	88.3096%	96.9314%
RKPM	74.3174%	93.5920%	98.4111%
Mix RKI	74.0020%	93.6215%	98.4354%

The displacement error norms of the proposed method using $\bar{R}_I = 1.2, 2.0, 3.0$ for $\bar{\Phi}_{\bar{a}_I}$ are shown in Figure 13, and the corresponding vertical displacement along $y = 0.0$ and shear stress distributions along $x = 5.0$ using finest discretization are plotted in Figures 14 and 15.

6.3. Two dimensional plate with hole

An infinite plate with a central circular hole (diameter 2a) subjected to a unidirectional tensile load 1.0 in the x direction as show in Figure 16 is studied using the proposed method. Plane strain condition is assumed with Young's modulus $E = 2.11 \times 10^{11}$ Pa and Poisson's ratio $v = 0.3$. The exact solution of this problem is given in the polar co-ordinates:

$$\sigma_{xx} = 1 - \frac{a^2}{r^2}\left(\frac{3}{2}\cos(2\phi) + \cos(4\phi)\right) + \frac{3a^4}{2r^4}\cos(4\phi)$$

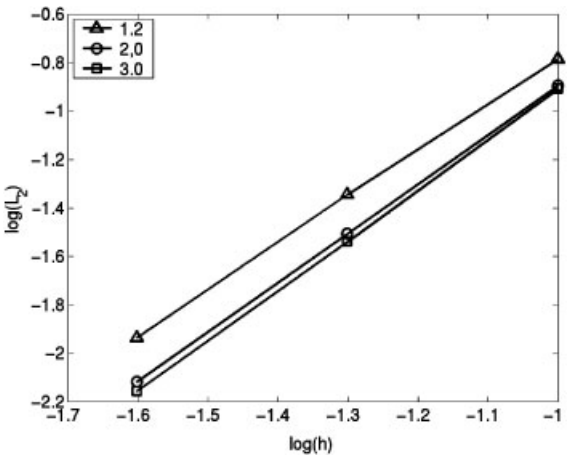

Figure 13. L_2 norm using $\bar{R}_I = 1.2, 2.0, 3.0$.

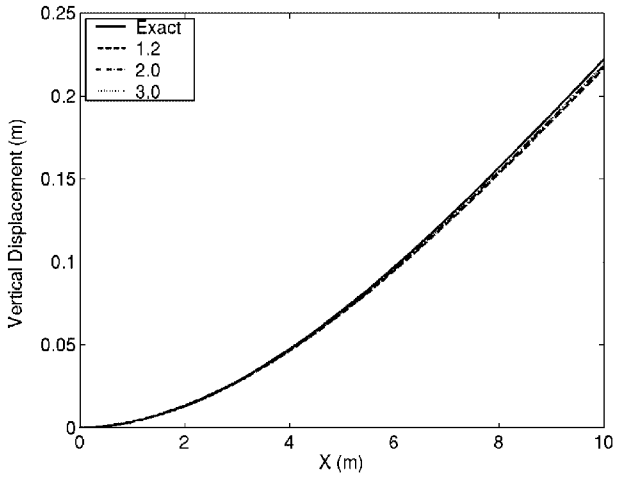

Figure 14. Vertical displacement $y = 0.0$ using $\bar{R}_I = 1.2, 2.0, 3.0$.

$$\sigma_{yy} = -\frac{a^2}{r^2}\left(\frac{1}{2}\cos(2\phi) - \cos(4\phi)\right) - \frac{3a^4}{2r^4}\cos(4\phi) \tag{86}$$

$$\tau_{xy} = -\frac{a^2}{r^2}\left(\frac{1}{2}\sin(2\phi) + \sin(4\phi)\right) + \frac{3a^4}{2r^4}\sin(4\phi)$$

where (r, ϕ) are the usual polar co-ordinates. Owing to geometric symmetry, only half model was modelled by three domain discretizations using 45, 153, and 561 points as shown in Figure 17. The traction along the edges $x = \pm 5$ and $y = 5$ are given according to the analytic solution Equation (86).

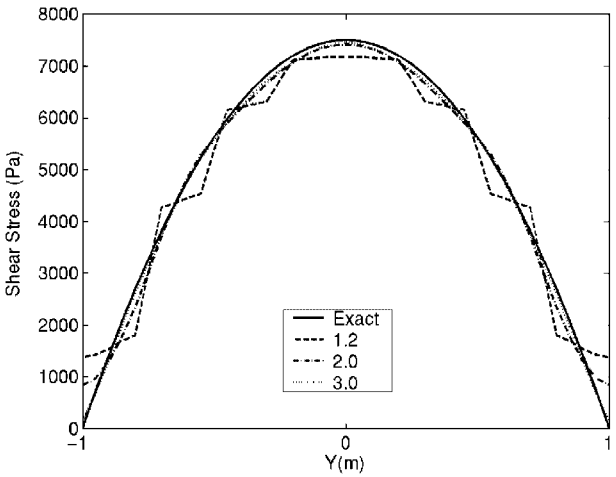

Figure 15. Shear stress along $x = 5.0$ using $\bar{R}_I = 1.2, 2.0, 3.0$.

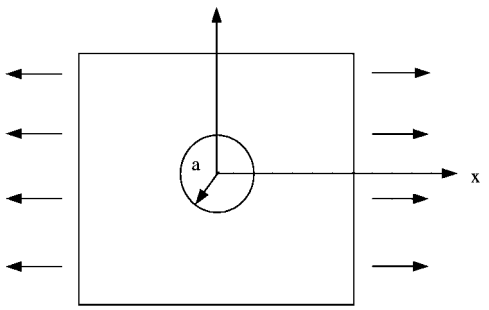

Figure 16. Problem statement: $a = 1$, and plate dimension is 10×10.

The normal stresses σ_{xx} along the line $x = 5$ using the Mixed RKI with three discretizations are presented in Figure 18. Results comparison using the Mixed RKI and the conventional RK approximation with the finest discretization is shown in Figure 19, and the corresponding energy norms are compared in Figure 20.

7. CONCLUSIONS

A general formulation for constructing meshfree interpolation functions that preserve reproducing conditions is presented. It is based on a coupling of a primitive function and an enrichment function. The primitive function introduces Kronecker delta properties, while the enrichment function is responsible for meeting reproducing conditions. By enforcing reproducing conditions on the combined shape function, an orthogonality condition at nodal points exists between the vector of the enrichment functions and the vector of shifted monomial

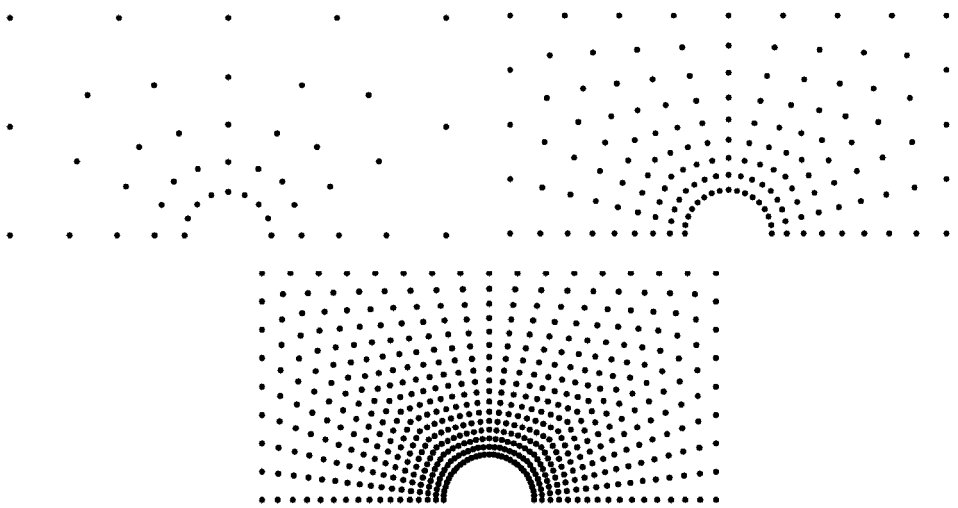

Figure 17. Domain discretization with 45, 153 and 561 nodes.

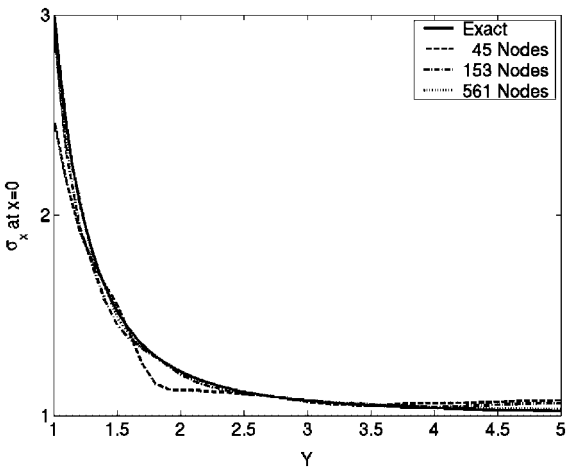

Figure 18. Stress plot along $x = 0$ for 3 models using Mix RKI.

functions. It is shown that if the enrichment basis functions and the monomial basis functions form a regular pair, the orthogonality condition leads to a nullity of the enrichment function at nodal locations. As a consequence, the RK shape function becomes an interpolation function.

Based on this result, a RK interpolation function is constructed by coupling a nodal Kronecker delta primitive function and an enrichment function that takes the form of RK approximation. The nodal Kronecker delta function can be easily constructed by normalizing any kernel functions used in the RK approximation with the restricted support size so that it does not cover any neighbour points. This primitive function can be flexibly added to selected points or to all points for desired interpolation properties. For points with added

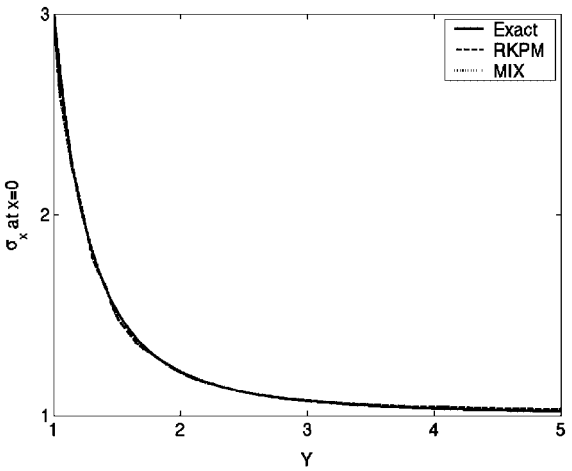

Figure 19. Stress comparison between RKPM and Mix RK interpolation.

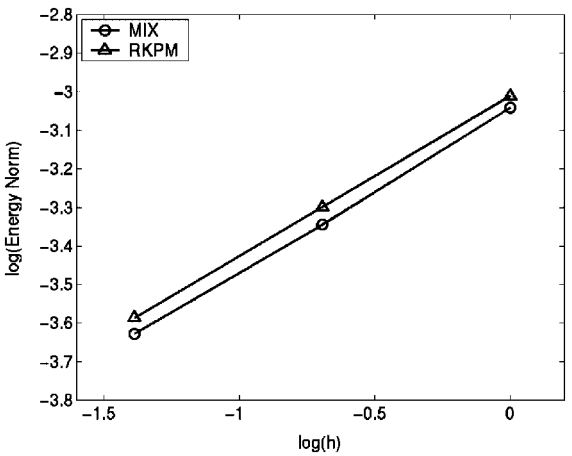

Figure 20. Energy norm comparison between RKPM and Mix RKI.

primitive functions, the coefficients of the corresponding RK shape functions become nodal values. This provides a convenient means for imposing essential boundary conditions. Optimal-order error estimates are shown rigorously for the proposed RK interpolant in any Sobolev norms. Optimal order convergence is maintained when the method is employed to solve one-dimensional boundary value problems. In two-dimensional problems, the order of convergence is not optimum for higher order basis. This is due to the fact that the essential boundary conditions are imposed only at discrete points. Similar phenomenon was observed in the meshfree solution using standard RK approximation.

When the primitive functions are selected to be the finite element shape functions, the proposed method reduces to the approach by Huerta *et al.* [17], in which a background grid

was needed. Since finite element shape functions are linearly complete, the basis functions in the enrichment function have to be at least second order. The smoothness of the resulting shape function is governed by the smoothness of the finite element shape function which is generally C^0. In the proposed method, since the proposed primitive function is merely a normalized kernel function, basis functions with arbitrary order can be used in the enrichment function. The continuity of the resulting shape function is the minimum continuity of the primitive and enrichment functions. Therefore, taking the same kernel function for primitive and enrichment functions leads to a shape function that has the same smoothness as the two component functions. Of course specific continuity in the primitive function can be chosen for particular applications.

The major advantage of the proposed method resides on its simplicity in dealing with essential boundary conditions or point loads without finite element enrichment. When a full RK interpolation is employed, the rate of convergence is slightly lower than that of the regular RK approximation. On the other hand, a mixed interpolation by introducing primitive functions only to the essential boundary points allows the standard treatment of essential boundary conditions while maintaining the good convergence properties of RK approximation. It should be noted that, although straightforward, the proposed RK interpolation only allows imposition of essential boundary conditions at nodal points. This is in contrast with the conventional finite element or coupling of finite element and meshfree methods. We are exploring the possibility of removing this drawback with new RK interpolations.

ACKNOWLEDGEMENTS

The support of this work by NSF/DARPA OPAAL Program under grant DMS 98-74015 and Sandia National Laboratories under the grant 5015 to the University of Iowa and UCLA is greatly acknowledged.

REFERENCES

1. Lancaster P, Salkauskas K. Surfaces generated by moving least squares methods. *Mathematics of Computation* 1981; **37**:141–158.
2. Nayroles B, Touzot G, Villon P. Generalizing the finite element method: diffuse approximation and diffuse elements. *Computational Mechanics* 1992; **10**:307–318.
3. Belytschko T, Lu YY, Gu L. Element-free Galerkin methods. *International Journal for Numerical Methods in Engineering* 1994; **37**:229–256.
4. Belytschko T, Kronggauz Y, Organ D, Fleming M. Meshless methods: an overview and recent developments. *Computer Methods in Applied Mechanics and Engineering* 1996; **139**:3–47.
5. Melenk JM, Babuska I. The partition of unity finite element method: basic theory and applications. *Computer Methods in Applied Mechanics and Engineering* 1996; **139**:289–314.
6. Babuska I, Melenk JM. The partition of unity method. *International Journal for Numerical Methods in Engineering* 1997; **40**:727–758.
7. Duarte CAM, Oden JT. A h-p adaptive method using clouds. *Computer Methods in Applied Mechanics and Engineering* 1996; **139**:237–262.
8. Liu WK, Jun S, Zhang YF. Reproducing kernel particle methods. *International Journal for Numerical Methods in Fluids* 1995; **20**:1081–1106.
9. Liu WK, Jun S, Li S, Adee J, Belytschko B. Reproducing kernel particle methods for structural dynamics. *International Journal for Numerical Methods in Engineering* 1995; **38**:1655–1679.
10. Liu WK, Li S, Belytschko T. Moving least square kernel Galerkin method. Part I. Methodology and convergence. *Computer Methods in Applied Mechanics and Engineering* 1997; **143**:422–433.
11. Zhu T, Atluri, SN. A modified collocation and a penalty formulation for enforcing the essential boundary conditions in the element free Galerkin method. *Computational Mechanics* 1998; **21**:211–222.
12. Chen JS, Pan C, Wu CT, Liu WK. Reproducing kernel particle methods for large deformation analysis of nonlinear structures. *Computer Methods in Applied Mechanics and Engineering* 1996; **139**:195–227.

13. Kaljevic I, Saigal S. An improved element free Galerkin formulation. *International Journal for Numerical Methods in Engineering* 1997; **40**:2953–2974.
14. Chen JS, Wang HP. New boundary condition treatments for meshless computation of contact problems. *Computer Methods in Applied Mechanics and Engineering* 2000; **187**:441–468.
15. Gunther F, Liu WK. Implementation of boundary conditions for meshless methods. *Computer Methods in Applied Mechanics and Engineering* 1998; **163**:205–230.
16. Krongauz Y, Belytschko T. Enforcement of essential boundary conditions in meshless approximations using finite elements. *Computer Methods in Applied Mechanics and Engineering* 1996; **131**:133–145.
17. Huerta A, Fernández-Méndez S. Enrichment and coupling of the finite element and meshless methods. *International Journal for Numerical Methods in Engineering* 2000; **48**:1615–1636.
18. Wagner GJ, Liu WK. Hierarchical enrichment for bridging scales and meshfree boundary conditions. *International Journal for Numerical Methods in Engineering* 2001; **50**:507–524.
19. Han W, Wagner GJ, Liu WK. Convergence analysis of a hierarchical enrichment of dirichlet boundary conditions in a meshfree method. *International Journal for Numerical Methods in Engineering* 2002; **53**:1323–1336.
20. Beissel S, Belytschko T. Nodal integration of the element-free Galerkin method. *Computer Methods in Applied Mechanics and Engineering* 1996; **139**:49–74.
21. Bonet J, Kulasegaram S. Correction and stabilization of smooth particle hydrodynamics methods with applications in metal forming simulation. *International Journal for Numerical Methods in Engineering* 2000; **47**:1189–1214.
22. Chen JS, Wu CT, Yoon S, You Y. A stabilized conforming nodal integration for Galerkin mesh-free methods. *International Journal for Numerical Methods in Engineering* 2001; **50**:435–466.
23. Han W, Meng X. Error analysis of the reproducing kernel particle method. *Computer Methods in Applied Mechanics and Engineering* 2001; **190**:6157–6181.
24. Brenner SC, Scott LR. *The Mathematical Theory of Finite Element Methods*. Springer: New York, 1994.

